Benchmarking GEANT4 nuclear models for hadron therapy with 95 MeV/nucleon carbon ions

J. Dudouet,* D. Cussol, D. Durand, and M. Labalme
LPC Caen, ENSICAEN, Université de Caen, CNRS/IN2P3, Caen, France
(Received 4 March 2014; revised manuscript received 21 April 2014; published 29 May 2014)

In carbon therapy, the interaction of the incoming beam with human tissue may lead to the production of a large amount of nuclear fragments and secondary light particles. An accurate estimation of the biological dose on the tumor and the surrounding healthy tissue thus requires sophisticated simulation tools based on nuclear reaction models. The validity of such models requires intensive comparisons with as many sets of experimental data as possible. Up to now, a rather limited set of double differential carbon fragmentation cross sections has been measured in the energy range used in hadron therapy (up to 400 MeV/nucleon). However, new data have been recently obtained at intermediate energy (95 MeV/nucleon). The aim of this work is to compare the reaction models embedded in the GEANT4 Monte Carlo toolkit with these new data. The strengths and weaknesses of each tested model, i.e., G4BinaryLightIonReaction, G4QMDReaction, and INCL++, coupled to two different de-excitation models, i.e., the generalized evaporation model and the Fermi break-up model, are discussed.

DOI: 10.1103/PhysRevC.89.054616 PACS number(s): 25.70.Mn, 24.10.Lx

I. INTRODUCTION

The use of carbon ions in oncology is motivated by some ballistic and biological advantages. Carbon ions allow one to better target the tumor while preserving the surrounding healthy tissue. However, the physical dose deposition is affected by the inelastic processes of the ions along the penetration path in human tissue [1,2]. For instance, the number of incident ions reaching the tumor (at the Bragg peak depth) is reduced by up to 70% for 400 MeV/nucleon ^{12}C in tissue-equivalent material [3]. Carbon beam fragmentation in the human body leads to the production of secondary lighter fragments with larger ranges and larger angular spreads. Such fragments also have a different biological efficiency, which is strongly correlated to the linear energy transfer (LET). These effects, due to carbon fragmentation, result in a complex spatial dose distribution, particularly on healthy tissue. The influence of secondary particle production is the highest beyond the Bragg peak where only secondary particles contribute to the dose.

In view of the previous remarks, keeping the benefits of carbon ions in hadron therapy requires a very high accuracy on the dose deposition pattern (±3% on the dose value and ±2 mm spatial resolution [4]). In planning a tumor treatment, the nuclear reactions need to be correctly evaluated to compute the biological dose all along the beam path. Monte Carlo methods are probably the most powerful tools to take into account such effects. Even though they generally cannot be directly used in clinical situations because of the excessively long processing time, they can be used to constrain and optimize analytical treatment planning systems (TPSs) [5,6] or to generate complete and accurate databases [3,7–10].

The ability of Monte Carlo codes to reproduce differential yields of charged fragments from carbon fragmentation has been recently studied. Böhlen *et al.* [11] studied the prediction capability of FLUKA [12] and GEANT4 [13] for the fragmentation of primary 400 MeV/nucleon ^{12}C in a thick water target. This work has shown disagreement by up to 100% for the models provided by the GEANT4 toolkit (namely G4BinaryLightIonReaction and G4QMDReaction). Another comparison has been done using the GEANT4 toolkit for a 95 MeV/nucleon ^{12}C on thick PMMA ($C_5H_8O_2$) targets [14]. This study has shown discrepancies of up to an order of magnitude as compared to experimental data, especially at forward angles.

In view of this difficulty of the GEANT4 nuclear models to reproduce the fragmentation processes within the energy range useful in carbon therapy using thick targets, it appeared necessary to constrain these nuclear models with double differential fragmentation cross sections on thin targets. A first set of experimental data has been obtained for a 62 MeV/nucleon ^{12}C on a thin carbon target [10]. GEANT4 simulation results have shown discrepancies of up to one order of magnitude for both angular and energy distributions.

A new set of double differential cross section data have been recently obtained by our collaboration (LPC Caen, IPHC Strasbourg, SPhN Saclay, IPN Lyon, and GANIL). These data, described in Dudouet *et al.* [15], provide good quality measurements (within a 5% to 15% accuracy) of 95 MeV/nucleon ^{12}C differential cross sections on thin targets (C, CH_2, Al, Al_2O_3, Ti, and PMMA). These experimental data are used in this work to test the different nuclear models embedded in the GEANT4 framework. These nuclear models tested are the following: G4BinaryLightIonReaction, G4QMDReaction, and INCL++. They are coupled to two de-excitation models: the generalized evaporation model and the Fermi break-up model. Strengths and weaknesses of these different models in reproducing the fragment production yields, the angular and energy distributions, as well as the target mass dependence will be discussed.

II. MONTE CARLO SIMULATIONS

GEANT4 is a Monte Carlo particle transport code used to simulate the propagation of particles through matter by taking into account both electromagnetic and nuclear processes. It is widely used in a variety of application domains, including medical physics. The 9.6 version of GEANT4 has been used

*dudouet@lpccaen.in2p3.fr

in this work. Electromagnetic interactions are those developed in the "electromagnetic standard package option 3." Particle transport cuts have been set to 700 μm. Total nucleus-nucleus reaction cross sections have been determined, as recommended, using the recently implemented Glauber-Gribov model [16]. This model provides the full set of nucleus-nucleus cross sections needed for the GEANT4 tracking (inelastic, elastic, particle production, and quasi-elastic) for all incident energies above 100 keV/A.

Nuclear reactions are usually described by a two-step process: a first dynamical step called the "entrance channel" followed by a de-excitation step called the "exit channel." The entrance channel model describes the collision and the production of excited nuclear species until thermal equilibrium is achieved. The decay of such hot species is thus considered in a second step by means of statistical de-excitation models. All nuclear models implemented in GEANT4 follow this scheme. In this work, three different entrance channel models are coupled with two exit channel models, leading to six different combinations. We stress that the aim of this article is to provide a benchmark of nucleus-nucleus collision models as they are implemented in the GEANT4 toolkit, rather than to test the physical relevance of these models.

A. GEANT4 entrance channel models

Two nuclear models are currently recommended to perform simulations for hadron therapy. The first one is a binary intranuclear cascade (BIC) model called G4BinaryLightIonReaction [17]. This is an extension of the binary cascade model [18] for light-ion reactions. This model can be characterized as a hybrid model between a classical cascade code and a quantum molecular dynamics (QMD) description because the "participating" particles are described by means of Gaussian wave functions. "Participating" particles are those particles that are either primary particles from the projectile or particles generated and/or scattered during the cascade process. The Hamiltonian is built with a time-independent optical potential. This potential is acting on participants only. Note that, in this model, scattering between participants is not taken into account. Participants are tracked until escaping from the nucleus or until the end of the cascade. The cascade stops if the mean kinetic energy of participants in the system drops below 15 MeV or if all the participant kinetic energies are below 75 MeV. If such conditions are fulfilled, the system is assumed to have reached thermal equilibrium. The nuclear system is left in an excited state, the evolution of which toward equilibrium is described by the native pre-compound model of GEANT4.

Another model used in hadron therapy is a QMD-like model called G4QMDReaction [19] adapted from the JAERI QMD (JQMD) code [20,21]. As in the BIC model, the basic assumption of a QMD model is that each nucleon is described by a Gaussian wave function which is propagated inside the nuclear medium. Differently from the previous model, in the QMD model, all nucleons of the target and of the projectile are taken into account. Each nucleon is thus considered as a participant. The particles are propagated and interact by means of a phenomenological nucleon-nucleon potential. The time evolution of the system is stopped at 100 fm/c, where it is assumed that equilibrium has been achieved. The QMD model does not include a pre-compound model.

A third model has been used in this work: the Liège intranuclear cascade model INCL++ [17,22,23]. The latest version implemented in GEANT4 is labeled as INCL++ v5.1.8. This model has recently shown promising results [14] comparable with the BIC or QMD models. Nucleons are modeled as a free Fermi gas in a static potential well. To treat the collision, a target volume is first calculated. Nucleons from the projectile entering this volume are labeled as participants. The quasi-projectile is built from projectile spectators and from noncascading projectile participants. In contrast, the quasi-target is included in the calculation volume, which also encompasses the participant zone. The final state of the quasi-target is determined by the full collision dynamics of the cascade. Its physical description is therefore much more reliable. The nucleus-nucleus collision is thus not treated symmetrically. Results have shown that INCL better reproduces the target fragmentation than the projectile fragmentation [14]. In view of this, INCL treats by default the collision in inverse kinematics (target impinging on projectile), in order to obtain the best reproduction of the projectile fragmentation. However, INCL is not able to use projectiles heavier than $A = 18$. If the target is heavier than $A = 18$, the collision will then be performed in direct kinematics. If both target and projectile are heavier than $A = 18$, the description of the collision uses the G4BinaryLightIonReaction model. The effects of this asymmetry in the treatment of the projectile and the target and the discontinuity at mass 18 will be discussed later. The cascade is stopped when no participants are left in the nucleus or when a stopping time defined as $t_{\text{stop}} = 70 \times (A_{\text{target}}/208)^{0.16}$ fm/c is reached. As in the G4QMDReaction model, the INCL model does not include a pre-compound model.

For the QMD and INCL++ models, a clustering procedure is applied to nucleons. For the QMD model, this clustering procedure is made in phase space. For the INCL++ model, this clustering procedure is based on a coalescence model. The clustering procedure produces excited species at the end of the cascade. For the BIC model, no clustering procedure is applied and the excitation energies are determined for the projectile and the target remnants. The excitation energy of each species is then estimated and is the input for the de-excitation process considered in the statistical de-excitation codes.

B. GEANT4 exit channel models

GEANT4 provides several de-excitation models which have been recently improved [24]. These models describe particle evaporation from excited nuclear species produced in the entrance channel. Two models have been considered in this work.

The first one is the generalized evaporation model (GEM) [17,25]. Based on the Weisskopf-Ewing evaporation model [26], it considers sequential particle emission up to ^{28}Mg as well as fission and γ decay.

The second model is the Fermi break-up model (FBU) [17]. This model considers the decay of an excited nucleus into n stable fragments produced in their ground state or in low-lying discrete states. The break-up probabilities for each decay channel are first calculated by considering the n-body phase-space distribution. Such probabilities are then used to sample

TABLE I. Energy thresholds used in the simulations.

Isotope	^{1}H	^{2}H	^{3}H	^{3}He	^{4}He	^{6}He	^{6}Li	^{7}Li	
E_{th} (MeV)	4.0	5.2	6.1	14.2	16.0	18.6	29.9	31.7	
Isotope	^{7}Be	^{9}Be	^{10}Be	^{8}B	^{10}B	^{11}B	^{10}C	^{11}C	^{12}C
E_{th} (MeV)	44.3	48.6	50.5	60.6	65.8	68.1	81.3	84.2	86.9

the decay channels by a Monte Carlo procedure. This model is only used for light nuclei ($Z \leqslant 8$ and $A \leqslant 16$). For heavier nuclei, the de-excitation process is considered using the GEM.

III. EXPERIMENTAL DATA

The models described above will be compared with data obtained during the E600 experiment performed in May 2011 at the Grand Accélérateur National d'Ions Lourds (GANIL) facility. The experiment has allowed measurements of the double differential cross sections of various species in 95 MeV/nucleon ^{12}C reactions on H, C, O, Al, and ^{nat}Ti targets [15]. The description of the experimental setup and the experimental energy thresholds are described in Dudouet *et al.* [15]. The particles have been detected by using three-stage telescopes, located at angles ranging from 4° to 43°. They have been identified by using a ΔE-E method. The analysis method has been described in Dudouet *et al.* [27]. The errors bars of the presented experimental data include systematic and statistical errors.[1]

In the presented simulations, only the energy thresholds of the telescopes have been taken into account. As a reminder, these thresholds are shown in Table I for all the detected isotopes. The main effects of these thresholds is to lower the contribution of the particles coming from the target fragmentation. It has been verified that the presented simulations and the simulations in which the whole setup is taken into account give the same results. The main drawback of these latter simulations is their lack of CPU efficiency since the fragmentation process in thin targets is rare and the solid angles of detectors are small. The target thicknesses used in the simulations are the same as the experimental one in order to obtain the same angular and energy straggling. A total of 10^9 incident ^{12}C atoms have been used in the simulations in order to minimize the statistical error on the simulated data (which is lower than 1% in most cases but up to 20% for the larger angles). For clarity, the choice has been made to not represent the statistical errors of the simulated data.

[1]These data are available with free access from the following website: http://hadrontherapy-data.in2p3.fr.

IV. RESULTS

A. The participant-spectator scheme

Some characteristics of the results will be discussed in the framework of the participant-spectator picture of the collision (see, for instance, Fig. 1 [28,29]).

This is a typical high-energy process (in the GeV/A range) in which the internal velocities of the nucleons are (much) smaller than the relative velocity between the two partners of the reactions. However, recent analyses have shown that it could still be valid at incident energy of 100 MeV/nucleon [15]. In such a picture, for a finite impact parameter b, the nucleons located in real space in the overlapping region of the two nuclei constitute the "participants." The projectile nucleons outside the overlapping region constitute the moderately excited quasi-projectile moving with a velocity close to the beam velocity. The same argument applies for the target nucleons, leading to a quasi-target moving with a velocity close to 0. The participants constitute the so-called highly excited mid-rapidity source. The decay products from this source show an energy distribution shifted toward lower values as compared to the beam energy. Therefore, in such a picture, three energy contributions in the laboratory frame are expected: a first one close to the beam energy, a second one associated with the target at energies close to 0, and, in between, a contribution associated with the participants. This latter is thus to a large extent strongly coupled to the sizes of the projectile and of the target and should show up as the size of the target increases. We stress that this very simple picture is used here to define the terms that characterize the origins of the detected fragments and is not used as a realistic description of the reaction mechanisms.

The results of the models considered above are now compared with experimental data. We first consider a comparison of simulated cross sections (production yields and angular and energy distributions) with the experimental data in the case of a carbon target. Then, the target mass dependence will be studied.

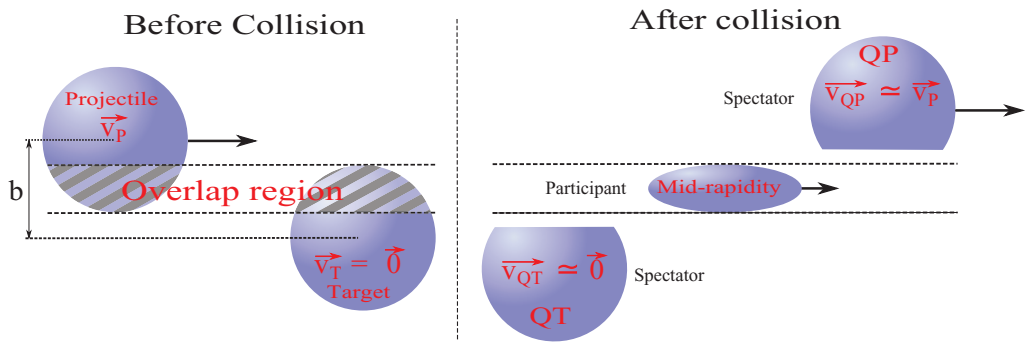

FIG. 1. (Color online) Schematic representation of the geometrical participant-spectator model in the laboratory frame.

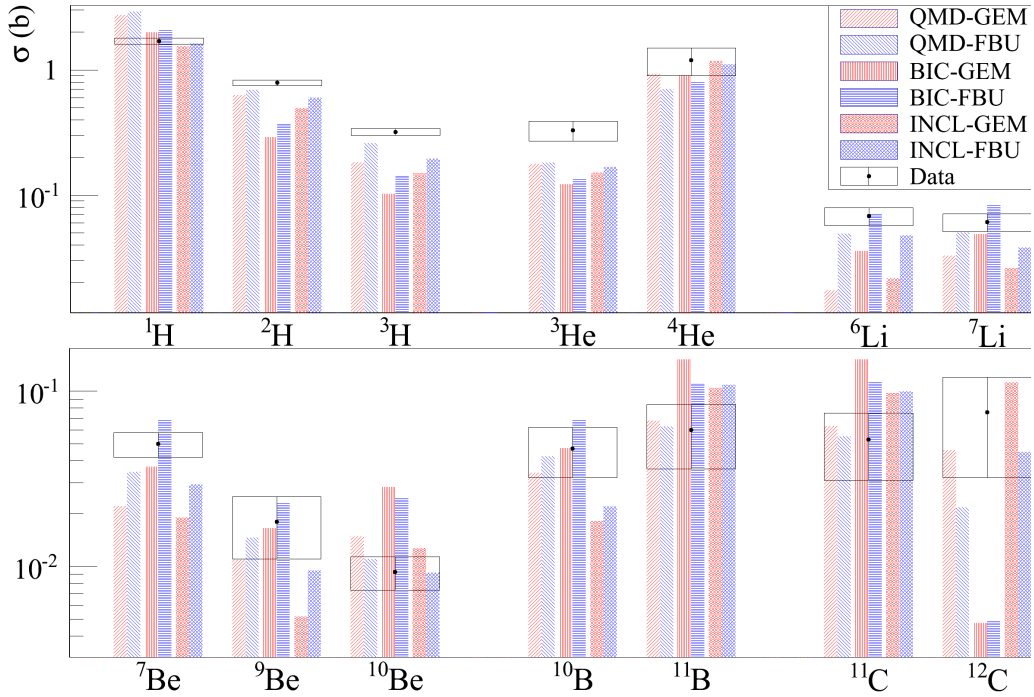

FIG. 2. (Color online) Comparisons between data and the different combinations of entrance and exit channel models (see text) for the production cross sections of various isotopes in 95 MeV/nucleon ^{12}C → ^{12}C reactions.

B. Production cross sections

Figure 2 displays the production cross sections of the most abundant reaction products in the case of a carbon target. They are compared with the GEANT4 results with different combinations between the entrance and exit channel models discussed previously. Note that the production cross section of ^{12}C fragments takes into account only inelastic interactions, excluding elastic scattering. These production cross sections have been obtained by fitting the angular distributions with a function resulting from the sum of a Gaussian and an exponential function. These fitted functions have then been integrated over the whole solid angle [15]. The errors bars represented on Fig. 2 have been obtained by propagating the fit parameters uncertainties, using the covariance matrix of the fit procedure.

The results of Fig. 2 clearly show that none of the model combinations can reproduce the production rates for all isotopes. Moreover, it is not easy to identify which model combination is the most suited for a comparison with experimental data. However, it may be concluded that the influence of the entrance channel is larger than the influence of the exit channel model. Regarding the two exit channel models, the FBU model seems, for a given entrance channel model, to be, in most cases, more compatible with the data. This was already mentioned in Böhlen *et al.* [11] and Ivanchenko *et al.* [30]. This is due, to some extent, to the fact that the FBU description allows one to explore more available phase space [especially at high excitation energies for which three (or more) body decays may play an increasing role] than the GEM for which only sequential evaporation is taken into account. In the following, we only consider calculations in which the FBU model is used for the exit channel.

C. Angular distributions

The E600 experimental setup allowed angular coverage ranging from 4° to 43° by steps of 2°. Figure 3 displays the differential angular cross sections for a carbon target for both experimental data and simulations using QMD, BIC, and INCL models coupled with the FBU de-excitation model.

Although the QMD model is the best model for describing the dynamics of the collision, it fails to reproduce the angular distributions. It strongly overestimates the proton production by about 50% (as also observed in Fig. 2) and poorly reproduces the angular distributions of the heavier isotopes considered here (by up to one order of magnitude). The distributions obtained with the QMD model show maximum values of around 7° (apart for protons) with a falloff toward 0°. This is in disagreement with the experimental distributions, which show an increase at very low angles.

The distributions obtained with the BIC model are slightly closer to the data as compared with the QMD results, especially at forward angles and for heavier fragment distributions (^{6}Li and ^{7}Be). The lack of α particles at forward angles may possibly come from a failure of the model to take into account the ^{12}C three-α cluster structure. The global shape is however not correct. The quasi-projectile contribution is too large and the large angles are poorly reproduced. The angular distributions obtained with the BIC model increases around 25° (except for protons). This probably comes from the quasi-target contribution but is in disagreement with experimental data.

Finally, INCL is the model that seems to better reproduce the angular distributions, especially for light fragments. The shapes of protons and α distributions are nearly reproduced

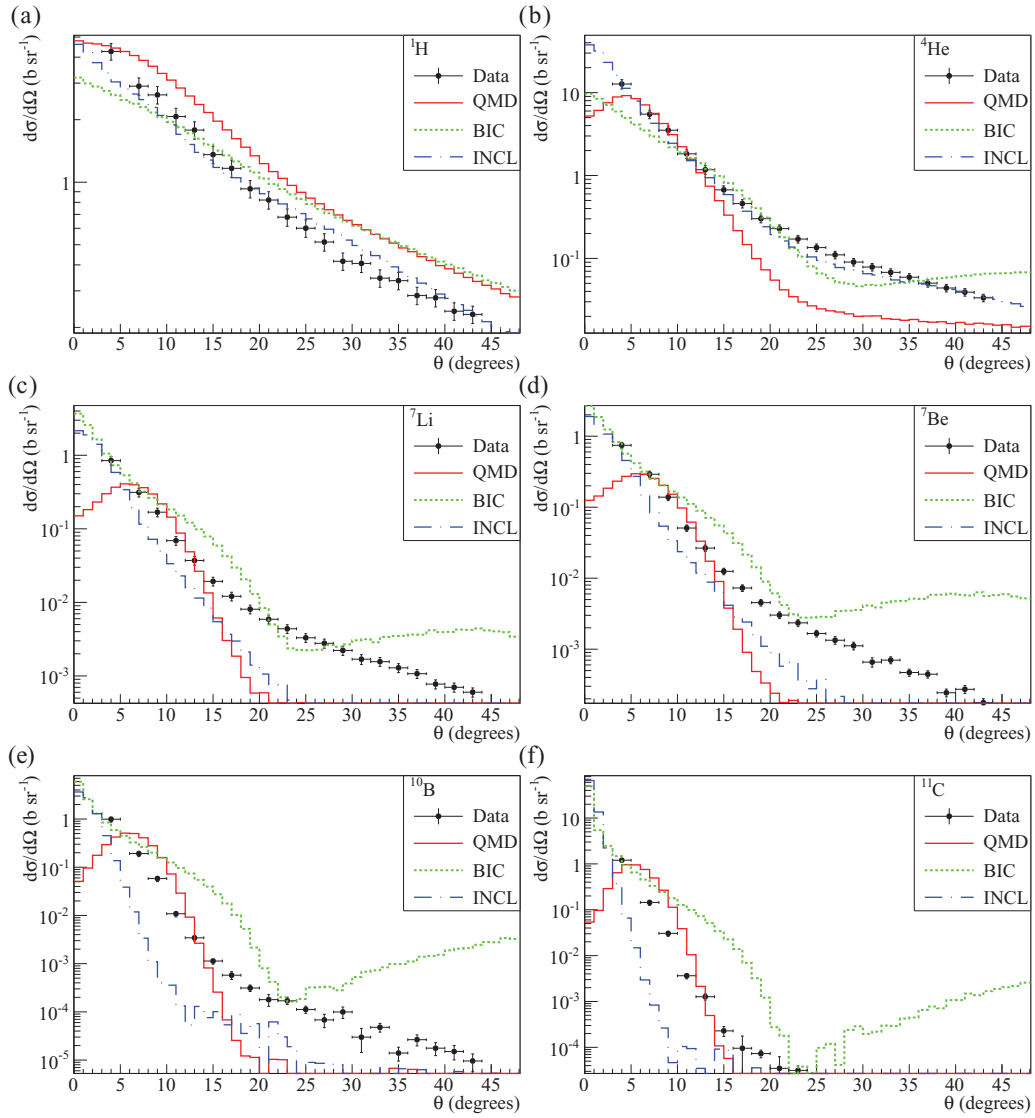

FIG. 3. (Color online) Absolute differential angular cross sections of protons, ^{4}He, ^{6}Li, ^{7}Be, ^{10}B, and ^{11}C obtained for the carbon target. Experimental data are indicated by black points. Histograms represetn GEANT4 simulations with QMD, BIC, and INCL models coupled to the FBU de-excitation model as indicated in the insets.

over the whole angular range (∼10%–20%), despite a small underestimation of the protons at forward angles. Regarding the distributions of heavier fragments, as with the BIC model, only the forward angles are well described. At large angles the INCL model strongly underestimates the data (by up to one order of magnitude).

We have shown in Dudouet *et al.* [15] that the experimental angular distributions of particles emitted in the 95 MeV/nucleon ^{12}C reaction on H, C, O, Al, and ^{nat}Ti can be represented as the sum of a Gaussian and an exponential contribution. None of the models used here are able to reproduce this trend. The main problem is associated with the inability of such models to reproduce the magnitude of the exponential contribution, which is dominant at large angles. Since this contribution is mostly resulting from the mid-rapidity source discussed previously, it is tempting to conclude at this stage that the present models do not contain the ingredients needed to describe the mid-rapidity processes. We now proceed with the energy distributions.

D. Energy distributions

The agreement with the double differential cross sections constitutes the most severe test of the models. Figure 4 shows a few examples of energy distributions obtained for ^{4}He, ^{6}Li, and ^{7}Be at 4° and 17°.

Here, we would like to focus on the shape of the distributions rather than on the absolute magnitude. The distributions may be interpreted as follows: The major contribution originates from the decay of the quasi-projectile and is thus located at an energy close to the beam energy per nucleon. This peak close to the beam energy is clearly visible at small angles (cf. Fig. 4, the distributions at 4°). At larger angles, this contribution tends to vanish because of the strong focusing of

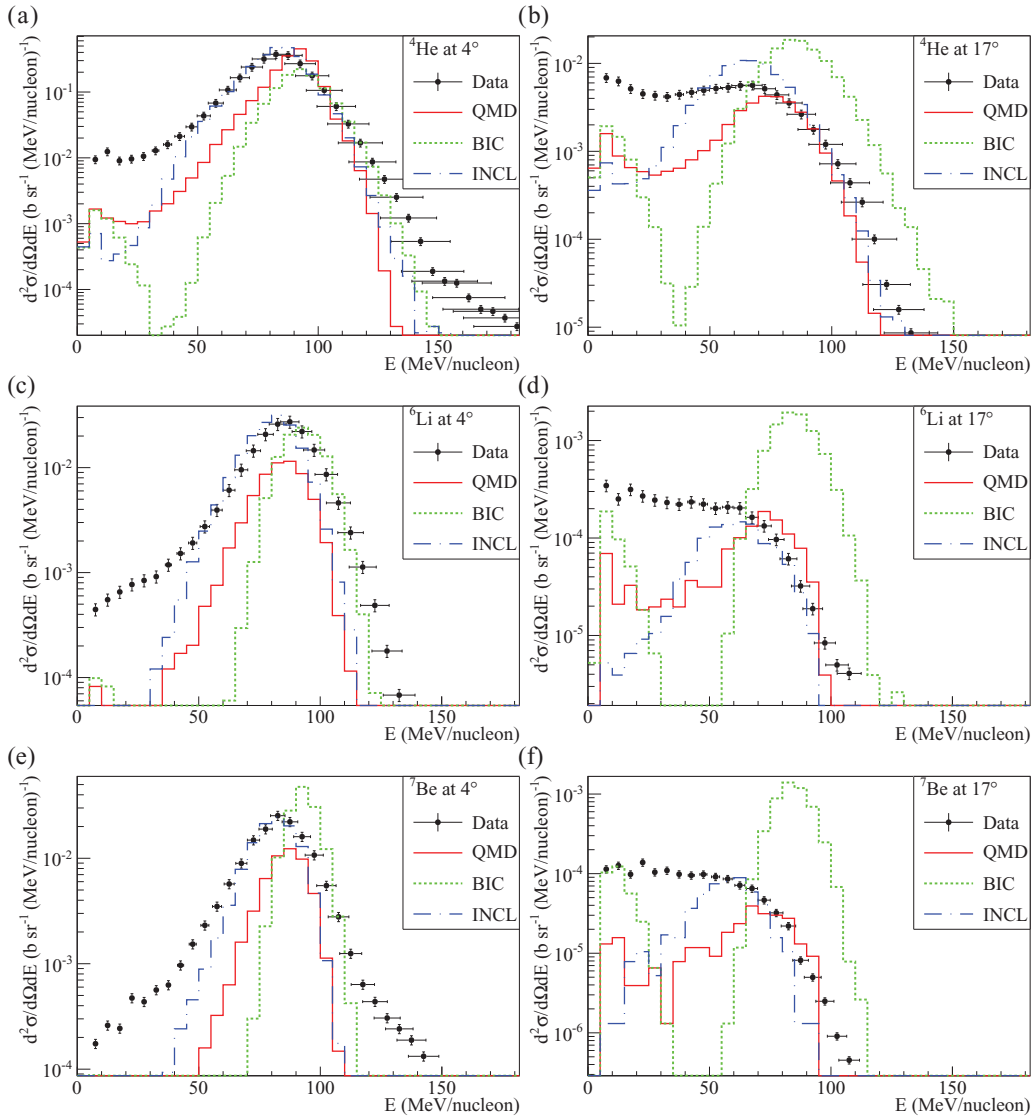

FIG. 4. (Color online) Energy distributions of ^{4}He, ^{6}Li, and ^{7}Be fragments at 4° and 17°. Black points are experimental data. Histograms are for simulations with QMD, BIC, and INCL models coupled to the FBU de-excitation model (see insets).

the quasi-projectile. The low-energy part of the distribution is associated with the species produced at mid-rapidity and also with the decay of the quasi-target, although this last contribution becomes dominant only at very large angles and can only be poorly detected owing to experimental energy thresholds. Therefore, the ability of the models to reproduce the data can be appreciated based on these two physical aspects: the decay of the quasi-projectile and the particle production mechanism at mid-rapidity.

As shown in Fig. 4, among the three models, BIC shows the strongest disagreement with the experimental data. In particular, the model is unable to account for the mid-rapidity contribution (medium angles). This is due to the binary nature of the reaction mechanism assumed in the model. Indeed, composite fragments cannot be formed in this model, and only nucleons undergoing nucleon-nucleon collisions can be emitted. Moreover, the mean energy of the quasi-projectile contribution is too large as compared to data, and its contribution (close to 95 MeV/u) remains too important at large angles. This leads for instance to the very strong disagreement shown in Fig. 4(d) for ^{7}Be fragments at 17°.

The INCL model better reproduces the quasi-projectile contribution for both the mean and the width of the energy distribution. It also predicts more fragments at low energies ($0 < E < 50$ MeV/nucleon) as compared to the BIC model. However, the results still underestimate the data. Moreover, the shape of the distributions at low energies (mid-rapidity contribution) is not in agreement with the data.

In contrast to the angular distributions, the QMD model better reproduces the global shape of the energy distributions. Although the mean energy of the quasi-projectile peak is slightly too high, the shape of the mid-rapidity contribution is better reproduced than in the BIC or INCL models. However, as in other models, it underestimates the mid-rapidity contribution.

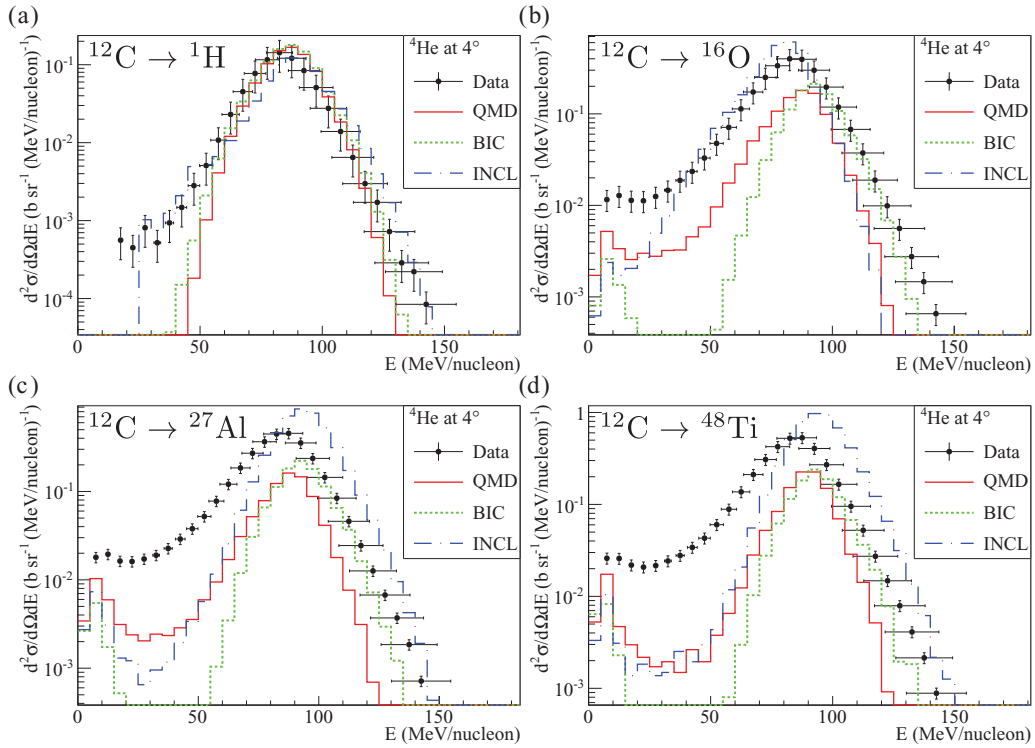

FIG. 5. (Color online) Energy distributions of α particles at 4° for hydrogen (a), oxygen (b), aluminum (c), and titanium (d) targets. Black points are experimental data. Histograms are simulations (see insets).

The remarks mentioned above are valid for all fragments from protons to carbon isotopes. The main conclusion that can be drawn is that none of the tested models can reproduce simultaneously the quasi-projectile, the quasi-target, and the mid-rapidity contributions. The INCL model better reproduces the quasi-projectile contribution: It is probably the best model for the description of the quasi-projectile. In contrast, the QMD model better describes the mid-rapidity emission, probably because it is the only model to take into account the time propagation and the interaction of all the nucleons in the reaction. Similar conclusions have been drawn at lower energy by De Napoli *et al.* [10], who tested the BIC and QMD models in 62 MeV/nucleon $^{12}C \rightarrow {}^{12}C$ induced reactions.

E. Results with other targets

Our experiment allowed us to gather data for a series of targets ranging from hydrogen up to titanium. The target dependence on the double differential cross sections is now investigated. Figure 5 displays the α energy distributions at 4° for the hydrogen, oxygen, aluminum, and titanium targets for both data and simulations using QMD, BIC, and INCL models coupled to the FBU de-excitation model.

The three models reproduce quite well the data for the hydrogen target, especially INCL. This result is not surprising in the sense that these models are mostly based on the concept of nuclear cascade, which was originally dedicated to nucleon-nucleus collisions. In such reactions, the geometry of the collision is rather simple and the description of the quasi-projectile is simpler than for nucleus-nucleus reactions. Moreover, with the hydrogen target, the α particles are mainly produced by the quasi-projectile de-excitation. However, the experimental data exhibit a small contribution at low energy (below 50 MeV/nucleon) and INCL is the only model to reproduce this contribution.

Nevertheless, the heavier the target, the larger the disagreement between the simulations and the experimental data. From carbon to titanium, the three models reproduce quite well the quasi-target and the quasi-projectile contributions. The difficulty in producing mid-rapidity fragments is evident. The discrepancy is amplified as the target mass increases, emphasizing the increasing role of mid-rapidity in the data as a simple consequence of the geometry of the reaction. The larger the mass of the target, the larger the size of the mid-rapidity region. The BIC model does not produce mid-rapidity fragments (around $E = 40$–50 MeV/nucleon). Although the situation is slightly better for INCL or QMD models, the mid-rapidity contribution is underestimated by both models.

Particular attention needs to be paid to the INCL model. For the aluminum and titanium targets, the shape of the energy distribution changes with respect to lighter targets. The projectile contribution is overestimated and the mean energy is too large. The reason for this is due to the discontinuity in the treatment of the kinematics when the target is larger than $A = 18$, as mentioned in Sec. II A. Otherwise, for lighter targets, results concerning the quasi-projectile are promising while the production at mid-rapidity remains underestimated.

In the participant-spectator reaction mechanism, the mid-rapidity contribution originates from the overlap region, as already mentioned previously. This is thus a geometrical contribution, which increases significantly with the target size, as it is observed experimentally when going from hydrogen to titanium targets: More and more fragments are produced in the

low-energy region. The three models that have been used here fail in accurately reproducing this region and the discrepancy increases with the mass of the target. This may be because none of them take accurately into account the possibility of producing sizable clusters in the overlapping region. This point deserves additional studies.

V. CONCLUSIONS

In this work, comparisons have been performed between experimental data collected in 95 MeV/nucleon ^{12}C reactions on H, C, O, Al, and ^{nat}Ti targets and GEANT4 simulations in order to test the models embedded in the GEANT4 nuclear reaction package. The G4BinaryLightIonReaction, G4QMDReaction, and INCL++ entrance channel models have been coupled to the generalized evaporation model and the Fermi break-up model exit channel models.

The main conclusion is that, up to now, none of these six model combinations is able to accurately reproduce the data, neither in term of production rates nor for angular or energy distributions.

This study has shown that the entrance channel model characteristics have a larger effect on production of particles and fragments as compared to the choice of the exit channel description. However, the FBU de-excitation model seems to give better results than the GEM. This observation has also been made by Böhlen *et al.* [11] and Ivanchenko *et al.* [30].

For angular distributions, apart from INCL, which reproduces quite well protons (with a small disagreement at forward angles) and α distributions for the carbon target, the models are not able to reproduce the data. The QMD model is the worst, with a maximum value of the distribution at around 7° and an unexpected falloff toward 0°.

In contrast, the QMD better reproduces the energy distributions for all considered fragments. Apart from the hydrogen target, the BIC model fails to reproduce the data and, in particular, it does not produce particles at low energy. The INCL model reproduces very well the quasi-projectile contribution if the target is not larger than $A = 18$.

These results seem consistent with those observed at lower energy. Indeed, the GEANT4 simulations that have been done by De Napoli *et al.* [10] have shown that the angular distributions were better reproduced by the BIC model than the QMD model. Regarding the energy distributions, it has been shown that the QMD model better reproduces the shape of the distribution than the BIC one. The conclusions on the GEANT4 nuclear models that we have reached at 95 MeV/nucleon are thus in agreement with the one reached at lower energies. The better reproduction of carbon fragmentation processes for the QMD model than for the BIC one has also been observed on thick water targets at higher energies by Böhlen *et al.* [11]. However, no INCL simulations have been performed in these two studies.

Finally, a study of the target mass dependence shows that the three models do not succeed in reproducing realistically the production of species at mid-rapidity. Comparisons with a simple phenomenological model that takes into account the geometrical overlap region is planned in the near future.

[1] D. Schardt *et al.*, Adv. Space Res. **17**, 87 (1996).
[2] N. Matsufuji, A. Fukumura, M. Komori, T. Kanai, and T. Kohno, Phys. Med. Biol. **48**, 1605 (2003).
[3] E. Haettner, H. Iwaseand, and D. Schardt, Radiat. Prot. Dosim. **122**, 485 (2006).
[4] SFPM, *Société Française de Physique Médicale: Guide des bonnes pratiques de physique médicale* (EDP Sciences, Les Ulis, France, 2013).
[5] L. Sihver and Davide Mancusi, Radiat. Meas. **44**, 38 (2009).
[6] M. Krämer and M. Durante, Eur. Phys. J. D **60**, 195 (2010).
[7] T. Toshito *et al.*, Phys. Rev. C **75**, 054606 (2007).
[8] A. N. Golovchenko, J. Skvarč, N. Yasuda, M. Giacomelli, S. P. Tretyakova, R. Ilić, R. Bimbot, M. Toulemonde, and T. Murakami, Phys. Rev. C **66**, 014609 (2002).
[9] I. Schall *et al.*, Nucl. Instrum. Methods B **117**, 221 (1996).
[10] M. de Napoli *et al.*, Phys. Med. Biol. **57**, 7651 (2012).
[11] T. T. Böhlen, F. Cerutti, M. Dosanjh, A. Ferrari, I. Gudowska, A. Mairani, and J. M. Quesada, Phys. Med. Biol. **55**, 5833 (2010).
[12] G. Battistoni, F. Cerutti, A. Fassò, A. Ferrari, S. Muraro, J. Ranft, S. Roesler, and P. R. Sala, AIP Conf. Proc. **896**, 31 (2007).
[13] S. Agostinelli *et al.*, Nucl. Instrum. Methods A **506**, 250 (2003).
[14] B. Braunn, A. Boudard, J. Colin, J. Cugnon, D. Cussol, J. C. David, P. Kaitaniemi, M. Labalme, S. Leray, and D. Mancusi, J. Phys. (Paris): Conf. Ser. **420**, 012163 (2013).
[15] J. Dudouet *et al.*, Phys. Rev. C **88**, 024606 (2013).
[16] V. M. Grichine, Eur. Phys. J. C **62**, 399 (2009).
[17] *Geant4 Physics Reference Manual* (Version 9.6.0), Chapters 30, 33, 34, 36, and 38, 2012.
[18] G. Folger, V. N. Ivanchenko, and J. P. Wellisch, Eur. Phys. J. A **21**, 407 (2004).
[19] T. Koi, in *Joint International Conference on Supercomputing in Nuclear Applications and Monte Carlo 2010 (SNA + MC2010), Hitotsubashi Memorial Hall, Tokyo, Japan, October 17–21, 2010*, http://geant4.web.cern.ch/geant4/results/papers/QMD-MC2010.pdf.
[20] K. Niita, S. Chiba, T. Maruyama, T. Maruyama, H. Takada, T. Fukahori, Y. Nakahara, and A. Iwamoto, Phys. Rev. C **52**, 2620 (1995).
[21] K. Niita, S. Chiba, T. Maruyama, T. Maruyama, H. Takada, T. Fukahori, Y. Nakahara, and A. Iwamoto, JAERI-Data/Code 99-042, 1999.
[22] A. Boudard, J. Cugnon, J.-C. David, S. Leray, and D. Mancusi, Phys. Rev. C **87**, 014606 (2013).
[23] P. Kaitaniemi, A. Boudard, S. Leray, J. Cugnon, and D. Mancusi, in *Progress in Nuclear Science and Technology*, Vol. 2 (Atomic Energy Society of Japan, Tokyo, 2011), pp. 788–793.
[24] J. M. Quesada, V. Ivanchenko, A. Ivanchenko, M. A. Cortés-Giraldo, G. Folger, A. Howard, and D. Wright, in *Progress in Nuclear Science and Technology*, Vol. 2 (Atomic Energy Society of Japan, Tokyo, 2011), pp. 936–941.
[25] S. Furihata, Nucl. Instrum. Methods B **171**, 251 (2000).

[26] V. F. Weisskopf and D. H. Ewing, Phys. Rev. **57**, 472 (1940).
[27] J. Dudouet *et al.*, Nucl. Instrum. Methods A **715**, 98 (2013).
[28] D. Durand, E. Suraud, and B. Tamain, *Nuclear Dynamics in the Nucleonic Regime*, Series in Fundamental and Applied Nuclear Physics (IoP, Inst. of Physics Publ., London, 2001).
[29] R. Babinet, École Joliot-Curie de Physique Nucélaire, 1985, http://www.cenbg.in2p3.fr/heberge/EcoleJoliotCurie/coursJC/JOLIOT-CURIE%201982.pdf.
[30] A. V. Ivanchenko, V. N. Ivanchenko, J.-M. Quesada, and S. Incerti, Int. J. Radiat. Biol. **88**, 171 (2012).